

Topological patterning of interacting polymers

Ricardo Pablo Pedro,^{1,*} Jayson Paulose,^{2,3,*} Anton Souslov,^{2,4} Mildred Dresselhaus,⁵ and Vincenzo Vitelli^{2,4,†}

¹*Department of Chemistry, Massachusetts Institute of Technology, Cambridge, MA 02139, USA*

²*Instituut-Lorentz, Universiteit Leiden, 2300 RA Leiden, The Netherlands*

³*Departments of Physics and Integrative Biology,
University of California, Berkeley, CA 94709, USA*

⁴*The James Franck Institute and Department of Physics,
The University of Chicago, Chicago, IL 60637, USA*

⁵*Department of Physics and Department of Electrical Engineering and Computer Science,
Massachusetts Institute of Technology, Cambridge, MA 02139, USA*

Polymer chains confined to a substrate show promise as a tool for nanoscale architecture, with applications ranging from anti-reflection coatings to oriented nanowires [1]. However, the desired control of polymer orientation is hard to achieve at the nanoscale [2–5]. In this Letter, we illustrate how a collective orientation can emerge among interacting polymer chains influenced by a spatially modulated substrate potential while experiencing strong thermal fluctuations. The resulting polymer orientation is tilted by an angle proportional to an integer topological invariant (the Chern number [6]) and hence is robust against substrate disorder, as demonstrated by Langevin dynamics simulations. We establish the topological underpinning of the tilted polymeric pattern via a correspondence between equilibrium polymer configurations and Thouless pumping [7] of a quantum Mott insulator in imaginary time. More generally, our strategy illustrates how to construct topologically protected gapped states in soft matter systems described by the diffusion equation with the addition of many-body interactions.

Here, we apply our framework to a system of directed polymers, which are linear polymer chains subject to a tension τ along the direction y . We assume that the polymers are confined to the xy -plane (Fig. 1a). Recent experimental advances have demonstrated that nanoscale control of chemical substrate patterning can induce polymer-substrate interactions with a desired potential energy $V(x, y)$ per unit length [2–5], which influences the equilibrium monomer density distribution (Fig. 1b). We aim to characterize the equilibrium polymer patterns induced by doubly periodic substrate potentials. Although the underlying principle is more general, we focus here on the specific form [8, 9]

$$V(x, y) = V_1 \cos\left(\frac{2\pi q}{a}x\right) + V_2 \cos\left(\frac{2\pi p}{a}x - \frac{2\pi}{\lambda}y\right), \quad (1)$$

which combines a y -independent sinusoidal component

(first term) with a mixed one (second term) which slides along the x -direction as y advances (Fig. 1c). The period in the x -direction is given by a divided by the greatest common divisor of the integers p and q , and in the y -direction the period is denoted by λ . (V_1 and V_2 are substrate energy scales.) The form of the potential in Eq. (1) is motivated by an analogy between the polymer system and the so-called Thouless charge pump [7], which was recently realized and extended in ultracold atom experiments [10–12].

A quantum Thouless pump describes the adiabatic flow of charge in a one-dimensional electron gas subject to a potential that varies periodically in both space and time. When the electrons populate an energy band completely, the number of electrons transported in one cycle is quantized to an integer-valued topological invariant of the filled band—the Chern number, \mathcal{C} . The static potential in Eq. 1 can be viewed as a time-dependent potential with the spatial coordinate y interpreted as the time coordinate. For electrons experiencing this potential, the Chern numbers are determined by the integers p and q [13] and can be nonzero, leading to charge flow. For the potential in Fig. 1 with $(p, q) = (1, 2)$, the lowest band has $\mathcal{C} = 1$. Hence, under a filling density of one electron per lattice period a , the electrons are shifted to the *right* by one lattice period over one time cycle λ , see Fig. 2a. By contrast, Fig. 2b illustrates the case $(p, q) = (2, 3)$, for which $\mathcal{C} = -1$. In this case, the electrons flow to the *left* even though the potential is still sliding to the right. As long as the gap between occupied and unoccupied bands remains open, the topological nature of \mathcal{C} insures that the charge flow is robust against electron interactions and disorder in the potential $V(x, y)$ [14].

Can Thouless pumping inspire the engineering of topological soft materials? Here, we show that polymer chains can order into tilted patterns that mimic the spacetime paths traced by the quantum particles in Fig. 2. Several studies have shown that the conformations of a thermally fluctuating chain can be mapped to the paths of a quantum particle [15–20]. However, Thouless pumping introduces a new facet to this mapping: the requirement of a gapped phase. For electrons, the gapped phase is accomplished by filling a band, which requires Pauli exclusion—a distinctive feature of fermions. To recreate

* These authors contributed equally to this work.

† vitelli@uchicago.edu

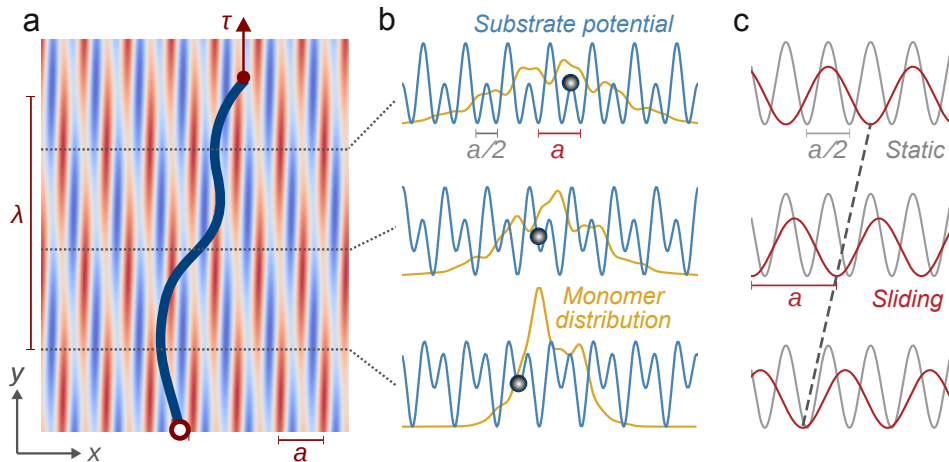


FIG. 1. **A directed polymer on a doubly-periodic substrate potential.** **a**, Schematic of a single directed polymer (thick curve) on top of a substrate potential (background) described by Eq. (1). The polymer is pinned at the bottom end and subjected to a tension τ along y at the top end. Shown is the case $(p, q) = (1, 2)$ and $\lambda > 0$, for which the lattice constant is a . **b**, In thermal equilibrium, the chain position at a given value of y fluctuates along x to produce a density distribution influenced by the substrate potential. Shown are the substrate potential (blue curves) and the theoretical density distribution (yellow curves) for a single polymer chain at three y -positions indicated by the dotted lines. The density distribution is obtained by solving the diffusion equation, Eq. (2), initialized with a delta function at the pinning point. **c**, The compound potential $V(x, y)$ (blue) combines two components, one of which (gray) is static with wavelength $a/q = a/2$ whereas the other (red) has wavelength $a/p = a$ and is translated along x as y changes, as tracked by the dashed line.

exclusion effects in classical polymers, we exploit the fact that polymer chains cannot cross. Remarkably, the non-crossing constraint reproduces the effects of Fermi statistics in the polymer system [15], allowing us to “fill” bands by tuning the number of chains per lattice constant along the x -direction.

To test whether an interacting, thermal polymer system can replicate topological charge pumping, we have conducted Langevin dynamics simulations of collections of polymer chains interacting with each other via a harmonic contact repulsion and, in addition, interacting with the substrate according to Eq. (1) with V_1 and V_2 of the same order as the thermal energy $k_B T$. (Simulation details are provided in SI.) We emulate filling of the lowest band by including polymers at a density of one chain per lattice constant a . When parameters $(p, q) = (1, 2)$ are chosen so that $\mathcal{C} = 1$, polymer chains acquire a collective tilt to the right (Fig. 3a) which is also apparent in the equilibrium density profile (Fig. 3b). Probability distributions of the monomer x -positions at different values of y show that the shift in average chain position advances to the right by one lattice constant per cycle, matching the quantization expected from the Chern number to within 1% accuracy (Figs. 3c–d).

In contrast to the quantum pump, the topological polymer tilt is a direct consequence of many-body interactions between the polymer chains: a single polymer on an otherwise empty lattice diffuses freely through the system and, on average, does not tilt, see Supplementary Movie for an illustration. Moreover, thermal fluctuations do not destroy the topological state, but rather are crucial for creating the tilt via a series of “thermal tunneling” events

visible in the density profiles of Fig. 3c. These events are analogous to the quantum tunneling in Fig. 2.

The non-vanishing slope resulting whenever $\mathcal{C} \neq 0$ cannot be intuited from superficial aspects of the substrate potential or from the (real-time) dynamics of classical particles under the same potential. For instance, Fig. 3e–h shows the case $(p, q) = (2, 3)$, for which $\mathcal{C} = -1$. Surprisingly, the polymer lines tilt to the left even though the sliding part of the potential, given by the last term in Eq. (1), has the positive slope $a/(\lambda p)$ which by itself would suggest a tilt to the right. Note that the topologically distinct left- and right-leaning configurations can be differentiated by their diffraction patterns (Figs. 3b and 3f, insets), suggesting a scattering experiment that would directly measure the underlying topological index.

To rigorously establish the topological origin of the observed tilt, we turn to the aforementioned mathematical correspondence between quantum particles and thermally fluctuating polymer lines [15–23]. This quantum-classical correspondence stems from the formal similarity between the Schrödinger equation and the diffusion equation describing polymer statistics:

$$\partial_y \Psi = \frac{k_B T}{2\tau} \partial_x^2 \Psi - \frac{1}{k_B T} V \Psi \equiv H \Psi. \quad (2)$$

Interpreted using the polymer language, Eq. (2) describes the (real) probability distribution $\Psi(x, y)$ of chain location x at distance y from the constrained end at $y = 0$, given the initial distribution $\Psi(x, 0)$. [The external tension prevents directed polymer chains from doubling back on themselves, which means that the instantaneous chain configurations are described by single-valued functions

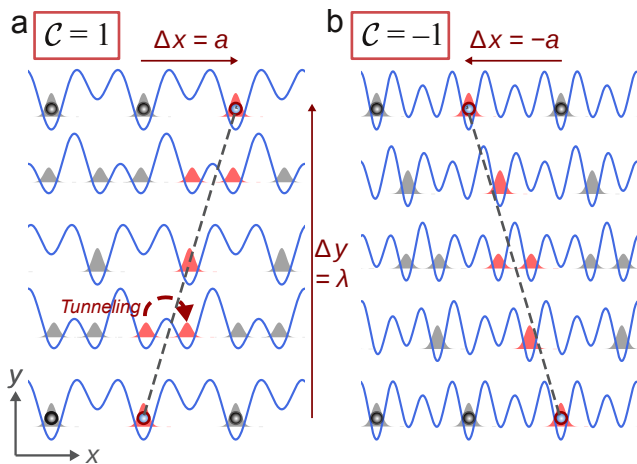


FIG. 2. **Thouless pumping of electrons.** **a**, Illustration of a quantum Thouless pump for a potential with $(p, q) = (1, 2)$, corresponding to $C = 1$. Under a filling density of one electron per lattice constant, each electron is exponentially localized to a unique unit cell. The drift of one such localized wavefunction over an adiabatic cycle is shown schematically; it is exactly quantized to C steps of lattice size a over each period λ of the potential variation along the y direction. The tunneling of probability weight between adjacent potential minima during the adiabatic evolution, indicated by the dashed arrow, is crucial for the shift. **b**, Same as **a** for a potential with $(p, 1) = (2, 3)$ for which $C = -1$.

$x(y)$.] On the other hand, upon equating y with it and $k_B T$ with \hbar , Eq. (2) describes the evolution of the (complex) wavefunction $\Psi(x, t)$ for a particle of mass τ in the time-dependent potential $V(x, t)$. For long polymers, a condition known as *ground-state dominance* guarantees that the solutions to Eq. (2) are described by the ground-state wavefunction of the analogous quantum system, see SI.

Interpolymer interactions can give rise to a gapped state. To see this, consider the y -evolution of the joint probability distribution of x -positions $\{x_0(y), x_1(y), \dots, x_N(y)\}$ of N chains in a y -independent potential $V(x)$, such as the potential in Eq. (1) when $V_2 = 0$. This many-body probability is described via the exchange-symmetric eigenstates of the effective Hamiltonian H in Eq. (2), augmented by a pair interaction term of the form $\beta \sum_{i < j} V_p(x_i - x_j)$. These (bosonic) many-body eigenstates may be challenging to describe. However, a tremendous simplification exists for non-crossing directed polymers, for which the pair potential is infinitely large when the positions of two polymers coincide at any y and is zero otherwise: $V_p = c\delta(x_i - x_j)$, $c \rightarrow \infty$. In this case, there is a one-to-one mapping between the requisite exchange-symmetric polymer eigenstates and the many-body wavefunctions of N noninteracting *fermions* confined to the x -axis and experiencing the same substrate potential $V(x)$ [15, 24]. In particular, if the number of polymers is equal to the number of lattice periods, the ground state is obtained by filling up

the lowest band entirely. This trivial electronic insulator in the fermion picture describes a Mott insulator in the polymer picture: a state in which excitations are gapped by virtue of interactions. The many-body joint probability distribution of the polymer system Ψ_0^P is then equal to the *absolute value* of the fermionic ground state Ψ_0^F [15, 19, 24].

When this gapped state is subject to an additional y -dependent potential, such as the V_2 term in Eq. (1), we can construct an insulating topological state [25] of the polymer system. In this state, the tilt of each polymer chain $\Delta\langle x \rangle_n$ relative to the tension direction y is given by the expression (see SI for a derivation):

$$\frac{\Delta\langle x \rangle_n}{a} = \frac{1}{2\pi} \int_0^\lambda dy \int_0^{\frac{2\pi}{a}} dk \mathcal{F}_n(y, k) \equiv C_n, \quad (3)$$

where $\mathcal{F}_n(y, k) = i(\langle \partial_y u_{k,n}(y) | \partial_k u_{k,n}(y) \rangle - \text{c.c.})$ is the Berry curvature of the n th band computed using the Bloch eigenstates $|u_{n,k}(y)\rangle$ of the Hamiltonian in Eq. (2) with the periodic potential $V(x, y)$ evaluated at a fixed y . While Eq. (3) is formally analogous to the electronic case, its applicability to polymeric systems is not trivial. It entails proving that even in *imaginary* time, the tilt $\frac{\Delta\langle x \rangle_n}{a}$ is equal to the Chern number. We establish this result in the SI by first constructing localized (i.e., Wannier) states that describe the single-polymer probability distributions at each y -slice. These states are similar to the single-electron wavefunctions shaded in each of the slices in Fig. 2. Next, we compute the y -dependence of the centres of mass for the local polymer states. This corresponds to tracking the time-evolution of electronic states as one moves along the vertical direction in Fig. 2. Finally, we show that the expectation value of the position operator can be computed using only the absolute value of the real-space representation of the fermionic states, $|\Psi_0^F|$. As a result, the relation between tilt and Chern number captured in Eq. (3) goes through unchanged under the polymer-fermion mapping $\Psi_0^P = |\Psi_0^F|$. While the Berry curvature is a property of the *complex* eigenstates of the Fourier-transformed Hamiltonian, the Chern number (i.e., integrated Berry curvature) describes the *real*-valued shift in the centres of mass of the single-polymer probability distributions.

An important property of adiabatic pumps is their robustness against disorder: since the shift in centres of mass of the single-particle states is associated with a topological index, it is unchanged by disorder in the substrate potential as long as the energy gap between the lowest and higher bands does not close [14]. To test the robustness of the polymer tilt, we add random noise to the substrate potential (implemented as a superposition of n_d sine functions with random amplitudes and phases, see Methods). Figs. 4a–b show a substrate potential with added disorder, and the corresponding equilibrium monomer density. The density profile in Fig. 4b looks substantially different from its crystalline counterpart in Fig. 3b. Nevertheless, the aggregated polymer

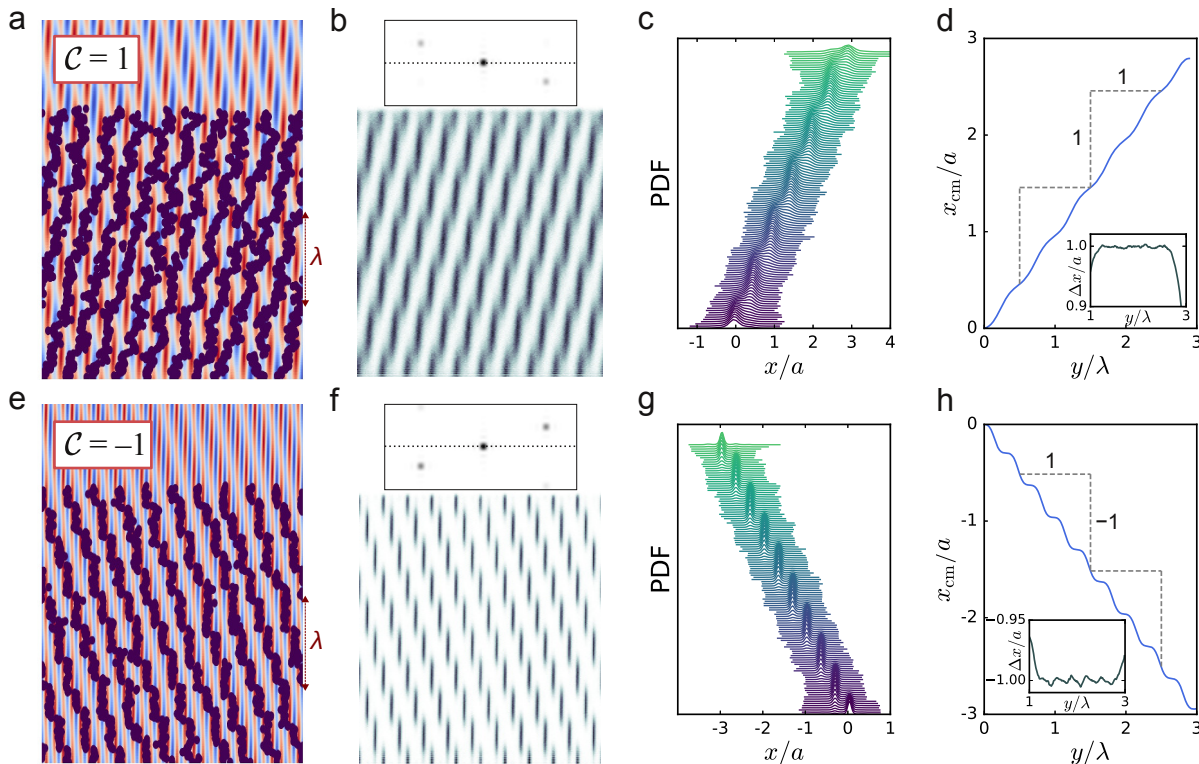


FIG. 3. **Topological tilt of polymer conformations.** **a**, Snapshot of a molecular dynamics simulation (see SI) of ten noncrossing directed polymer chains experiencing the substrate potential from Fig. 2a with $C = 1$ under commensurate filling (one chain per unit cell of the potential along the x direction). **b**, Equilibrium monomer density distribution, and numerically-computed scattering intensity profile (inset; see Methods). **c**, Probability distribution of monomer x -position for a subset of monomers along the length of the chains. Data from different chains are aggregated by first shifting the p th chain by an amount pa along x , where $p \in \{0, \dots, 9\}$ indexes the chains in order from left to right. **d**, Centre of mass computed from the probability distributions in **c**. The inset shows the shift over one period, $x_{\text{cm}}(y) - x_{\text{cm}}(y - \lambda)$, which agrees with the prediction of $C = 1$ away from the polymer ends. **e–h**, Same as **a–d** for the potential from Fig. 2b with $C = -1$.

tilt (Fig. 4c) shows a striking regularity. The measured slope of the equilibrium polymer conformations over one period (Fig. 4d) remains quantized by the Chern number until the disorder strength (the amplitude $|V_a|$ averaged over the substrate) becomes comparable to the energy gap E_g between the occupied band and the next-highest band in the energy spectrum.

The topological patterning is also robust against general interactions among polymer chains on top of the noncrossing constraint, which translate in the quantum language to many-body interactions (of the same functional form) among the fermions [24]. As with substrate disorder, the quantization is unaffected as long as the excitation gap remains open when the interactions are turned on [14]. This property is demonstrated by the results of our simulations that employ a harmonic contact potential (see SI).

In this work, we explored topological protection in polymer patterns, arising from a combination of strong interactions and equilibrium thermal fluctuations. Three ingredients are essential for implementing our model: (i) external tension (e.g., by immersing the polymers in a liquid-crystalline bath [16, 17, 26], or subjecting them

to strong electric or magnetic fields [27, 28]); (ii) confinement to a 2D substrate or interface (e.g., via a homogeneous chemical affinity or by being physically sandwiched); and (iii) periodic polymer-substrate interactions (e.g., via nanolithography [2–5]). We envision devices in which topological robustness in patterning may lead to polymer-based functionality despite manufacturing disorder at the nanoscale.

ACKNOWLEDGMENTS

We thank Benny van Zuiden for programming assistance, and Vadim Cheianov, Michel Fruchart, Alexander Grosberg, Charles L. Kane, Philip Pincus, D. Zeb Rocklin, and Tom Witten for insightful discussions. VV was primarily by the University of Chicago Materials Research Science and Engineering Center, which is funded by the National Science Foundation under award number DMR-1420709. JP acknowledges funding from NWO through a Delta ITP Zwaartekracht grant. RPP gratefully acknowledges the Office of Graduate Education of MIT for the graduate Unitech Blue Fellowship, and the

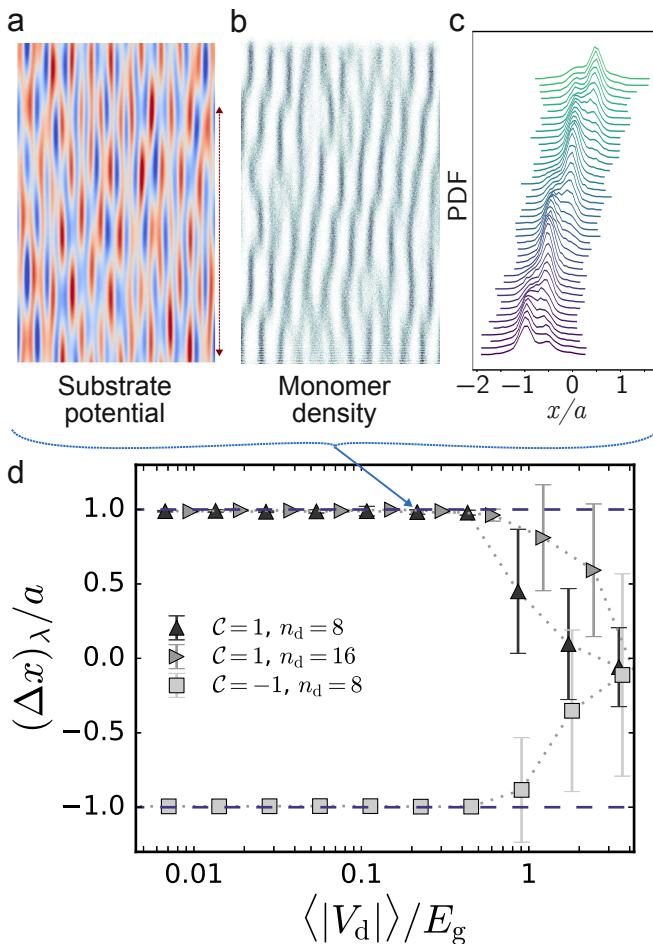


FIG. 4. **The polymer tilt is robust against disorder.** **a**, Example of a substrate potential with $\mathcal{C} = 1$ from Fig. 3a, with random disorder added. **b**, Equilibrium monomer density distribution for potential in **a** under commensurate filling. **c**, Aggregated probability density function of monomer x -positions. Although the density profiles of individual chains show deviations, the aggregated profile maintains the quantized tilt. **d**, Tilt as measured in simulations for increasing disorder added to the substrate interaction for the potentials studied in Fig. 3. Each point represents an average over ten realizations of random disorder; the error bars represent estimated standard deviations. Triangles and squares correspond to underlying periodic potentials with Chern numbers $\mathcal{C} = 1$ and -1 respectively, with n_d additional modes with random amplitude and phase added on. The quantized tilt is preserved until the disorder strength $\langle |V_d| \rangle$ becomes comparable to the excitation gap E_g .

King Abdullah University of Science and Technology for support under contract (OSR-2015-CRG4-2634).

Appendix A: Methods

1. Simulation details

We performed 2D molecular dynamics simulations in which polymer chains are approximated as chains of N beads of mass m connected by nonlinear springs with equilibrium length l_0 and maximum extension l_{\max} , implemented using the pair potential

$$V_{\text{chain}}(r) = -\frac{Kl_{\max}^2}{2} \log \left[1 - (r - l_0)^2 / l_{\max}^2 \right] \quad (\text{A1})$$

for linked beads with separation r . To implement the noncrossing constraint, each bead has a finite radius $r_c = l_0$ and interacts with all other beads via a harmonic contact potential $V_c(r) = k_c(r - l_0)^2$, $r < l_0$. Tension is applied by pulling the topmost bead along the y direction with a force τ . The bottom beads are either pinned to specific points with horizontal spacing a at $y = 0$ (for simulations in Fig. 1) or confined to $y = 0$ but free to slide along the x direction (for Figs. 2 and 3). The substrate interaction $V(x, y)$ per unit length is implemented as a position-dependent potential of strength $l_0 V(x, y)$ acting on every bead. For all simulations, we set $m = 1$, $l_0 = 0.3$, $K = k_c = 10^3$, $\tau = 10$, $a = 1$, $\lambda = 25$ in simulation units. The simulation box size is $L_x = 10a$ and $L_y = 16\lambda$ with periodic boundary conditions along x . The box size along y is always many times the polymer chain length.

Temperature is implemented by applying a friction force with drag coefficient γ to all beads, and adding a random force of strength $\sqrt{2\gamma k_B T}$ along each dimension to each bead. In all our simulations, we set $k_B T = 1$ and $\gamma = 0.5$ in simulation units. Newton's equations are solved using the velocity-Verlet algorithm with time steps of length 0.001 in simulation units, which equates to $0.0316/\omega$ where $\omega = \sqrt{k_c/m}$ is the contact-force time scale.

Simulations are initialized with straight, tension-free chains arranged parallel to the y axis and with horizontal spacing a along x . Each simulation is run for H time steps where H is of the order of 10^7 . To aid equilibration, simulations begin with an annealing phase in which the temperature is set to 2–3 times the desired temperature and reduced to the final temperature via a linear ramp in time for the first $H/2$ steps. Equilibrium quantities such as density profiles are measured from snapshots of the bead positions taken at every 1000 to 2000 time steps for the last quarter of the simulation.

Disorder is implemented by adding to the substrate potential a superposition of n_d products of sine functions with random amplitudes, wavelengths, and phases:

$$V_d = \sum_{i=1}^{n_d} \alpha_i \sin \left(\frac{2\pi r_i}{L_x} x + \phi_i \right) \sin \left(\frac{2\pi s_i}{L_y} y + \varphi_i \right), \quad (\text{A2})$$

where amplitude α_i is drawn from a normal distribution with zero mean and standard deviation $2\bar{V}_d/\sqrt{n_d}$, and

Simulation	Parameter	Value
Fig. 3, $\mathcal{C} = 1$	N	250
	H	2×10^7
	V_1	0.3333
	V_2	0.2333
Fig. 3, $\mathcal{C} = -1$	N	250
	H	4×10^7
	V_1	2
	V_2	0.8
Fig. 4, $\mathcal{C} = 1$	N	130
	H	5×10^7
	V_1	0.3333
	V_2	0.2333
Fig. 4, $\mathcal{C} = -1$	N	160
	H	8×10^7
	V_1	2
	V_2	0.8
Fig. A1	N	200
	H	2×10^8 (2×10^7) for panel b (c)
	V_1	0.0667
	V_2	0

TABLE I. Simulation parameters

random phases ϕ_i and φ_i are uniformly distributed in the interval $[0, 2\pi)$. To satisfy the periodic boundary conditions, the random wavelengths are integral fractions of the simulation box sizes (L_x, L_y) , with r_i and s_i drawn uniformly from integers in the intervals $5 \leq r_i \leq 20$ and $8 \leq s_i \leq 32$ respectively. In Fig. 3, we use $n_d = 8$ and 16.

Table I shows values of the situation-specific simulation parameters that have not been defined above.

2. Computing the scattering intensity profile

From the numerically averaged distribution of polymer density, we compute the scattering intensity profile. This quantity is proportional to the static structure factor $S(\mathbf{k})$ for the wavevector \mathbf{k} . The characteristic features of the scattering profile are the nearest-neighbor polymer density peaks situated along the direction separating the polymer chains (i.e., the direction perpendicular to the average polymer orientation). These peaks are signatures of orientational order in the polymer liquid, and can be compared to the peaks observed in X-ray scattering profiles for nematic or smectic liquid crystals. Numerically, we compute the scattering intensity by taking the Fourier transform of the density-density correlation function, i.e., we compute $\langle \rho(\mathbf{k})\rho(-\mathbf{k}) \rangle$. We plot the results in Figs. 3b,f of the main text.

Appendix B: Mapping polymer probability distributions to quantum-mechanical wavefunctions

The probability distribution $\Psi(x_1, y|x_0, 0)$ describing the statistical weight of a polymer chain with ends fixed at $x(0) = x_0$ and $x(y) = x_1$ can be expressed in terms of path integrals as

$$\Psi(x_1, y|x_0, 0) = \int_{x(0)=x_0}^{x(y)=x_1} \mathcal{D}\{x(y)\} \exp(-\beta E[x(y)]), \quad (\text{B1})$$

where the line energy E is a functional of $x(y)$ of the form

$$E = \int dy \left[\frac{\tau}{2} \left(\frac{dx(y)}{dy} \right)^2 + V[x(y)] \right]. \quad (\text{B2})$$

Upon discretizing the path integral above, the Schrödinger-like equation governing the change in partition weights due to the addition of a small element of length is given by Eq. (2) in the main text.

The many-body version of main text Eq. (2) is obtained by replacing the Laplacian operator ∂_x^2 with $\sum_i \partial_{x_i}^2$ and the potential $V(x)$ with a sum over pairs $\sum_{i<j} V(x_i - x_j)$.

1. Ground-state dominance and the polymeric Mott insulator

To further develop the polymer-quantum mapping, we formally express the solution to partition function evolution, Eq. (2), in terms of the eigenstates ψ_n and corresponding eigenvalues ε_n of H [18]:

$$\Psi(X_0, y|x_0, 0) = \langle X_0 | \left(\sum_n |\psi_n\rangle e^{-\beta \varepsilon_n y} \langle \psi_n | \right) | x_0 \rangle. \quad (\text{B3})$$

Here, the initial and final “wavefunctions” $|X_0\rangle$ and $|x_0\rangle$ are identified with the probability distributions of the polymer position at the initial and final locations: $|X_0\rangle = \delta(x - X_0)$ in the position basis. Equation (B3) highlights a crucial feature of the imaginary-time evolution: at long distances from the origin, all contributions to Ψ become exponentially small compared to the ground-state contribution. This situation, known as *ground state dominance*, simplifies the description of long directed polymers at equilibrium, which is completely captured by the ground state.

As an example of ground-state dominance for a single polymer, we consider the evolution in the probability density function of a single polymer, pinned at $(x_0, 0)$, in a periodic potential of the form $V(x) = V_1 \cos(2\pi x/a)$. The eigenstates of H are Bloch waves of the form $\psi_{nk}(x) = u_{nk}(x)e^{ikx}$, with cell-periodic functions $u_{nk}(x) = u_{nk}(x+a)$ of the same periodicity as the potential, and the normalization $\int dx \psi_{nk}^* \psi_{n'k'} =$

$(2\pi/a)\delta_{n,n'}\delta(k-k')$ for wavevectors belonging to the first Brillouin zone (BZ) $k, k' \in [-\pi/a, \pi/a]$. All real combinations of Bloch waves contribute to the probability evolution; the pinning condition corresponds to a delta-function probability distribution $\delta(x-x_0)$ represented as $\langle x|x_0 \rangle$, which has a nonzero overlap with eigenfunctions across the Brillouin zone. As y increases, however, the partition sum is dominated by states close to the ground state (red region in Fig. A1a, which is the $k=0$ eigenstate of the lowest band and therefore carries equal weight on all lattice sites. As a result, the polymer becomes more delocalized at larger y , as verified in simulations of a single polymer experiencing a periodic potential (Fig. A1b).

As described in the main text, noncrossing interactions among polymers can be exploited to prepare the polymer system in the analogue of a Mott-insulating state at a density of one polymer chain per lattice constant a . In the absence of any variation along the (imaginary) time axis, a signature of the Mott-insulating state is that polymers are confined to their respective potential wells due to repulsion with their neighbours. In Fig. A1c–d, we verify this fact for the y -independent potential. Simulations of a system of noncrossing polymers experiencing the same substrate potential as the single polymer in Fig. A1b, at the density needed to “fill” the lowest band, show that the noncrossing condition confines each polymer to its respective well (Fig. A1c), even though the depth of the wells was not sufficient to confine a single polymer (Fig. A1b). The diffusive evolution of the probability distribution with length for the lone polymer is overcome by polymer-polymer and polymer-substrate interactions under commensurate filling (Fig. A1d).

Appendix C: Many-body position operator for the polymer system

The concept of adiabatic pumping is closely connected to the modern theory of electronic polarization [29, 30], which builds on the realization that changes in polarization and associated current flows in an electronic system undergoing an adiabatic change are not captured by the expectation value of the ordinary position operator x which is ill-defined under periodic boundary conditions. However, they are captured by an appropriately-defined many-body position operator [31, 32],

$$\langle X \rangle = \frac{L}{2\pi} \text{Im} \ln \langle \Psi_0 | e^{i\frac{2\pi}{L} \sum_{i=1}^N x_i} | \Psi_0 \rangle, \quad (\text{C1})$$

where L is the system size.

Below, we apply this operator to the polymer system. First, let us provide a quantitative description of the Mott-insulating ground state using Wannier functions associated with the lowest band of the periodic potential. The Wannier functions, $W_{n,R}(x) = W_n(x-R)$ with $W_n(x) = \frac{a}{2\pi} \int_{\text{BZ}} dk \psi_{nk}(x) e^{-ikx}$, are a set of orthonormal basis functions for band n , each of which is associated

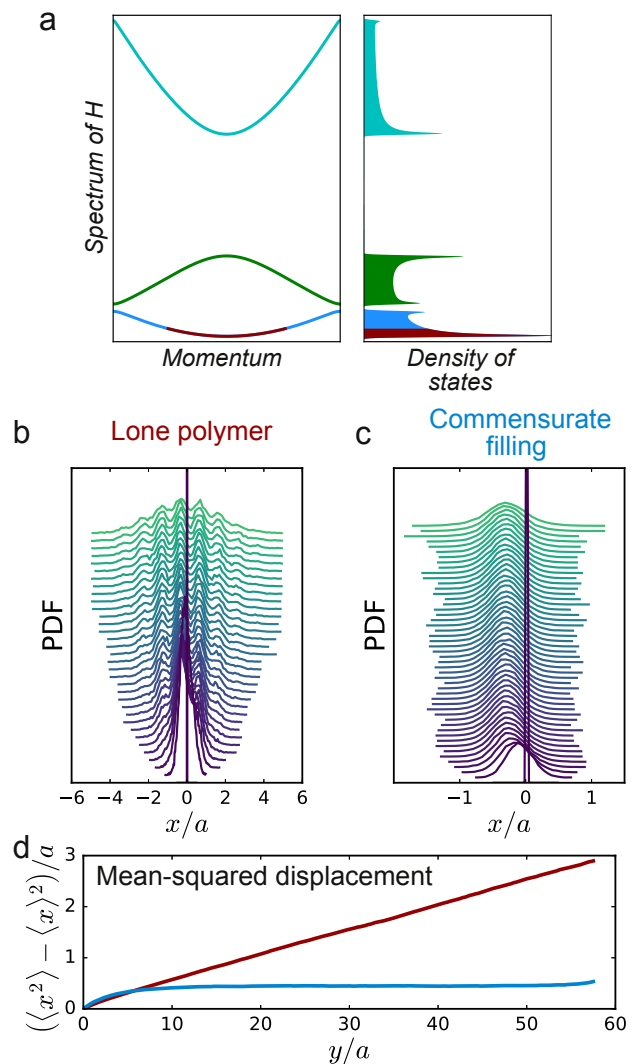


FIG. A1. **Mott insulator of noncrossing directed polymers on a periodic substrate.** **a**, Example of the single-particle band structure for a potential with $V_2 = 0$ which is constant along y , and exhibits gaps in the spectrum. The probability distribution of a solitary polymer is governed by states near the zero-momentum eigenstate of the lowest band (red area in **a**), and wanders over many lattice sites as shown by the spread of the probability density function of the chain position with distance from the pinning point (**b**). By contrast, under commensurate filling (having as many polymer chains as potential periods along x), the ground state of the analogous fermionic system is a completely filled lowest band (blue and red areas in **a** combined), which puts the system in a Mott-insulating state with polymers localized to individual potential valleys (**c**). **d**, The localization due to interactions in the many-polymer system (blue curve) tames the random-walk-like evolution of the position of a single polymer (red curve) as evidenced by the mean square displacement of monomer position as a function of distance y (which equates to time in the diffusion problem).

with a unit cell at lattice vector $R = ja$ and exponentially localized around it. For fermions, Wannier functions are not uniquely defined because of a gauge freedom in defining the cell-periodic Bloch eigenstates $|u_{n,k}(y)\rangle$, but a real set of Wannier functions can always be found for isolated bands in one-dimensional periodic potentials [33]. When the number of polymers equals the number of unit cells N , the fermionic ground state is obtained by assigning one polymer to each of the real Wannier functions spanning the lowest band $W_0(x - ja)$, $0 \leq j < N$, and computing a Slater determinant. The many-body ground state probability distribution of the polymer system is then the absolute value of the fermionic ground state [24]: $\Psi_0^P = |\Psi_0^F|$, where Ψ_0^P and Ψ_0^F denote the polymeric and fermionic ground-state wavefunctions respectively. As a result, the mapping from fermions to bosons preserves expectation values of operators that commute with the position wavefunctions.

Continuous changes in the substrate potential shift the centres of mass of the Wannier functions. A striking result underlying the modern theory of electronic polarization is that these shifts can be expressed in terms of Berry phases of the cell-periodic Bloch eigenstates of the corresponding bands [29, 30, 34]. As a result, when the underlying lattice Hamiltonian $H(x+a) = H(x)$ undergoes a periodic change along the y axis $H(x, y) = H(x, y + \lambda)$, the shift in centre of mass $\langle x \rangle_n = \int dx x W_{n,0}^2(x)$ of the $R = 0$ Wannier function over one period is a topological invariant built upon the Berry phase, quantized by the Chern number \mathcal{C}_n . Note that the Chern number describes

a shift in the centre of mass of the *real* Wannier functions which can be used to build the many-body states of the polymer system.

Now we show that the position operator in Eq. (C1) describes the flow of probability density of the polymer chain positions under the imaginary-time Schrödinger evolution, Eq. 2. For comparison to the quantum case, we use t in place of y as the coordinate along the tension direction. We work with eigenstates $\psi_n(x, t)$ of the ‘‘Hamiltonian’’ $\beta H = -[(1/2\tau\beta)\nabla^2 - \beta V]$. For convenience we set $\beta = 1$ in the remainder of this section. The Hamiltonian is real, and hence has a set of real orthonormal eigenstates at each time (instantaneous eigenstates) with corresponding eigenvalues ε_n :

$$H(t)\psi_n(t) = \varepsilon_n(t)\psi_n(t), \quad (\text{C2})$$

and $\langle \psi_m(t) | \psi_n(t) \rangle = \int dx \psi_m(x, t) \psi_n(x, t) = \delta_{mn}$. We drop the spatial coordinate x in what follows. If we begin with the decomposition $\Psi(t_0) = \sum_n a_n(t_0) \psi_n(t_0)$, then we can always find the eigenfunctions at all times $\psi_n(t)$, and the solution $\psi(t)$ can always be written as a superposition of these eigenfunctions, but the key to describing the evolution lies in finding the quantities $a_n(t)$.

We write the state at time t as

$$\Psi(t) = \sum_n a_n(t) \psi_n(t) e^{-\int_{t_0}^t \varepsilon_n(t') dt'}, \quad (\text{C3})$$

so that

$$\partial_t \Psi(t) = -H \Psi(t) \quad (\text{C4})$$

$$\Rightarrow \sum_n \left(-\varepsilon_n a_n \dot{\psi}_n + \dot{a}_n \psi_n + a_n \dot{\psi}_n \right) e^{-\int_{t_0}^t \varepsilon_n(t') dt'} = - \sum_n \varepsilon_n a_n \dot{\psi}_n e^{-\int_{t_0}^t \varepsilon_n(t') dt'} \quad (\text{C5})$$

$$\Rightarrow \sum_n \dot{a}_n \psi_n e^{-\int_{t_0}^t \varepsilon_n(t') dt'} = - \sum_n a_n \dot{\psi}_n e^{-\int_{t_0}^t \varepsilon_n(t') dt'}. \quad (\text{C6})$$

Using the orthogonality property, taking a dot product of the equation with ψ_m gives

$$\dot{a}_m = -a_m \langle \psi_m | \dot{\psi}_m \rangle - \sum_{n \neq m} a_n \langle \psi_m | \dot{\psi}_n \rangle e^{-\int_{t_0}^t (\varepsilon_n(t') - \varepsilon_m(t')) dt'}. \quad (\text{C7})$$

However, since we restrict ourselves to real orthogonal eigenstates, $\partial_t \langle \psi_m | \psi_m \rangle = 0 = \langle \dot{\psi}_m | \psi_m \rangle + \langle \psi_m | \dot{\psi}_m \rangle = 2 \langle \dot{\psi}_m | \psi_m \rangle \Rightarrow \langle \dot{\psi}_m | \psi_m \rangle = 0$. (In quantum perturbation theory, this condition would be imposed by a ‘‘parallel transport’’ gauge choice $\langle \psi_m | \dot{\psi}_m \rangle = 0$). Hence,

$$\dot{a}_m = - \sum_{n \neq m} a_n \langle \psi_m | \dot{\psi}_n \rangle e^{-\int_{t_0}^t (\varepsilon_n(t') - \varepsilon_m(t')) dt'}. \quad (\text{C8})$$

If we begin in the ground state: $a_0(t_0) = 1$, then to

lowest order we have $\dot{a}_0 = 0 \Rightarrow a_0(t) = 1$. However the coefficients of the excited states $m \neq 0$ have a lowest order contribution that is nonzero:

$$\dot{a}_m = - \langle \psi_m | \dot{\psi}_0 \rangle e^{-\int_{t_0}^t (\varepsilon_0(t') - \varepsilon_m(t')) dt'}. \quad (\text{C9})$$

with initial condition $a_m(t_0) = 0$. In the adiabatic limit where variations happen over a time scale $T \rightarrow \infty$, we are satisfied with a solution to the above equations for $a_m(t)$ to lowest order in $1/T$. We obtain this by integrating once by parts to get

$$a_m(t) \approx \frac{\langle \psi_m | \dot{\psi}_0 \rangle}{\varepsilon_0(t) - \varepsilon_m(t)} e^{-\int_{t_0}^t (\varepsilon_0(t') - \varepsilon_m(t')) dt'}. \quad (\text{C10})$$

The corrections to the above equations go as $\partial_t \langle \psi_m | \dot{\psi}_0 \rangle \sim \langle \psi_m | \dot{\psi}_0 \rangle / T$, and higher powers of $1/T$, as

required for accuracy in the adiabatic limit. Finally, the time-evolved wavefunction at all times can be written using Eq. C3 as

$$\Psi(t) = e^{-\int_{t_0}^t \varepsilon_0(t') dt'} \left(\psi_0(t) + \sum_{m \neq 0} \frac{\langle \psi_m | \dot{\psi}_0 \rangle}{\varepsilon_0(t) - \varepsilon_m(t)} \psi_m(t) \right). \quad (\text{C11})$$

At first glance, the time evolution of the ground state appears to depend on the lowest instantaneous eigenvalue. This is, however, an artifact: although the imaginary-time Schrödinger equation does not conserve probability, any computations involving the partition weight $\Psi(x, t)$ requires normalization by the partition sum $Z \equiv \int dx \Psi(x, t)$. Therefore, the overall magnitude of the time-evolved wavefunction is arbitrary and we may choose a factor that explicitly conserves net probability integrated over the span of the system:

$$\Psi(t) = \psi_0(t) + \sum_{m \neq 0} \frac{\langle \psi_m | \dot{\psi}_0 \rangle}{\varepsilon_0(t) - \varepsilon_m(t)} \psi_m(t), \quad (\text{C12})$$

for which $\langle \Psi | \Psi \rangle = 1 + O(1/T^2)$.

We are interested in the probability distribution of points in the interior of a directed polymer at $y = t$, far away from the ends at $y = 0$ and $y = L$, which is described purely by the ground state of the Hamiltonian regardless of pinning conditions. In addition to the partial partition weight $\Psi(x, t|x_0, 0)$ of finding the polymer at position x at y -coordinate t , we need to consider the weight $\Psi^\dagger(x, t|x_L, L)$ associated with conformations connecting the interior point at t to the pinning point at L . The complementary partition function is governed by the equation $-\partial_t \Psi^\dagger = [(1/2\tau\beta)\nabla^2 - \beta V]\Psi^\dagger = -\beta H \Psi^\dagger$. The dagger does not signify conjugation; Ψ and Ψ^\dagger are different functions. However the notation is suggestive and the situation parallels that of a wavefunction and its conjugate in the quantum mechanical picture. Repeating the time-dependent perturbation theory calculation provides the following expression for $\Psi^\dagger(t)$:

$$\Psi^\dagger(t) = \psi_0(t) - \sum_{m \neq 0} \frac{\langle \psi_m | \dot{\psi}_0 \rangle}{\varepsilon_0(t) - \varepsilon_m(t)} \psi_m(t), \quad (\text{C13})$$

The spatial density distribution at y -coordinate t is written as:

$$\rho(x, t) = \frac{1}{Z} \Psi(x, t|x_0, 0) \Psi^\dagger(x, t|x_L, L), \quad (\text{C14})$$

where $Z = \int dx \Psi(x, r_0; t) \Psi^\dagger(x, r_1; t) = \Psi(x_L, L|x_0, 0)$ is the full partition function of the chain and therefore independent of t . We can treat Z as a time-independent normalization, and we will not write it explicitly in what follows. The time evolution of the spatial density produces a ‘‘probability current density’’ j through the con-

tinuity equation

$$\partial_t \rho(x, t) + \partial_x j(x, t) = 0 \quad (\text{C15})$$

$$\Rightarrow \partial_x j = -\Psi \partial_t \Psi^\dagger - \Psi^\dagger \partial_t \Psi \quad (\text{C16})$$

$$= \frac{1}{2\tau\beta} (\Psi \partial_x^2 \Psi^\dagger - \Psi^\dagger \partial_x^2 \Psi) - \beta V (\Psi \Psi^\dagger - \Psi^\dagger \Psi) \quad (\text{C17})$$

$$\Rightarrow j = \frac{1}{2\tau\beta} (\Psi \partial_x \Psi^\dagger - \Psi^\dagger \partial_x \Psi). \quad (\text{C18})$$

(we reintroduce the general β from now on).

The shift in expected position of the polymer chain upon traversing a period T in ‘‘time’’ (i.e. distance along the chain) is now obtained by integrating the current density over a period and over all space. Substituting the perturbative expressions for Ψ and Ψ^\dagger into the current equation, we get

$$j(x, t) = \frac{1}{2\tau\beta} \sum_{m \neq 0} \frac{\langle \psi_m | \dot{\psi}_0 \rangle}{\varepsilon_0(t) - \varepsilon_m(t)} [2\psi_m \partial_x \psi_0 - 2\psi_0 \partial_x \psi_m]. \quad (\text{C19})$$

Integrating over space to get the average current, we have

$$J(t) = \frac{1}{L} \int dx j(x, t) = \frac{2}{\tau\beta} \sum_{m \neq 0} \frac{\langle \partial_x \psi_0 | \psi_m \rangle \langle \psi_m | \partial_t \psi_0 \rangle}{\varepsilon_0 - \varepsilon_m}, \quad (\text{C20})$$

where we have used the orthogonality $\langle \psi_m | \psi_0 \rangle = 0$ which implies $\langle \psi_m | \partial_x \psi_0 \rangle + \langle \partial_x \psi_m | \psi_0 \rangle = 0$.

Using the fact that the instantaneous eigenstates ψ_i can always be chosen to be real for real Hamiltonians, the right hand side of Eq. C20 may be written as

$$J(t) = \frac{1}{\tau\beta} \sum_{m \neq 0} \left(\frac{\langle \partial_x \psi_0 | \psi_m \rangle \langle \psi_m | \partial_t \psi_0 \rangle}{\varepsilon_0 - \varepsilon_m} + \frac{\langle \partial_t \psi_0 | \psi_m \rangle \langle \psi_m | \partial_x \psi_0 \rangle}{\varepsilon_0 - \varepsilon_m} \right), \quad (\text{C21})$$

Upon identifying the quantum-mechanical momentum operator p with $-i\hbar\partial_x$ and substituting $\hbar^2/2m$ for $1/2\tau\beta$, the right hand side of Eq. C21 is identical to the average flow of current under adiabatic evolution of a quantum electronic system with the same potential $V(x)$ [7, 14, 31], which forms the basis for the theories of polarization and quantized charge pumping. Furthermore, for adiabatic evolution of the Hamiltonian, the current is the time-derivative of the expectation value of the many-body position operator:

$$J(t) = \frac{1}{L} \frac{d}{dt} \langle X \rangle. \quad (\text{C22})$$

Like the position operator, the probability flow therefore depends only on the square modulus of the instantaneous ground-state wavefunction [31]. Since the instantaneous adiabatic ground states of the polymeric system are simply the absolute values of the corresponding ground states of the electron system and share the same form of

their probability evolution over time, the equivalence of the two problems has been established.

The equivalence of the probability current with the quantum-mechanical system and the existence of exponentially localized Wannier functions for the polymeric

system also provides a route to rigorously proving the robustness of the polymer tilt under many-body interactions and substrate disorder, following the techniques of Niu and Thouless [14].

-
- [1] Steve Granick, Sanat K Kumar, Eric J Amis, Markus Antonietti, Anna C Balazs, Arup K Chakraborty, Gary S Grest, Craig Hawker, Paul Janmey, Edward J Kramer, *et al.*, “Macromolecules at surfaces: Research challenges and opportunities from tribology to biology,” *Journal of Polymer Science Part B: Polymer Physics* **41**, 2755–2793 (2003).
- [2] Miri Park, Christopher Harrison, Paul M. Chaikin, Richard A. Register, and Douglas H. Adamson, “Block copolymer lithography: Periodic arrays of 1011 holes in 1 square centimeter,” *Science* **276**, 1401–1404 (1997).
- [3] Sang Ouk Kim, Harun H. Solak, Mark P. Stoykovich, Nicola J. Ferrier, Juan J. de Pablo, and Paul F. Nealey, “Epitaxial self-assembly of block copolymers on lithographically defined nanopatterned substrates,” *Nature* **424**, 411 (2003).
- [4] Dong Qin, Younan Xia, and George M. Whitesides, “Soft lithography for micro- and nanoscale patterning,” *Nature Protocols* **5**, 491 (2010).
- [5] Gurdaman S. Khaira, Jian Qin, Grant P. Garner, Shisheng Xiong, Lei Wan, Ricardo Ruiz, Heinrich M. Jaeger, Paul F. Nealey, and Juan J. de Pablo, “Evolutionary optimization of directed self-assembly of triblock copolymers on chemically patterned substrates,” *ACS Macro Letters* **3**, 747–752 (2014).
- [6] D. J. Thouless, M. Kohmoto, M. P. Nightingale, and M. den Nijs, “Quantized Hall Conductance in a Two-Dimensional Periodic Potential,” *Physical Review Letters* **49**, 405–408 (1982).
- [7] D. J. Thouless, “Quantization of particle transport,” *Physical Review B* **27**, 6083–6087 (1983).
- [8] Lei Wang, Matthias Troyer, and Xi Dai, “Topological Charge Pumping in a One-Dimensional Optical Lattice,” *Physical Review Letters* **111**, 026802 (2013).
- [9] Ran Wei and Erich J Mueller, “Anomalous charge pumping in a one-dimensional optical superlattice,” *Physical Review A* **92**, 013609 (2015).
- [10] Shuta Nakajima, Takafumi Tomita, Shintaro Taie, Tomohiro Ichinose, Hideki Ozawa, Lei Wang, Matthias Troyer, and Yoshiro Takahashi, “Topological Thouless pumping of ultracold fermions,” *Nature Physics* **12**, 296–300 (2016).
- [11] Michael Lohse, Christian Schweizer, Oded Zilberberg, Monika Aidelsburger, and Immanuel Bloch, “A Thouless quantum pump with ultracold bosonic atoms in an optical superlattice,” *Nature Physics* **12**, 350–354 (2015).
- [12] Michael Lohse, Christian Schweizer, Hannah M. Price, Oded Zilberberg, and Immanuel Bloch, “Exploring 4D quantum Hall physics with a 2D topological charge pump,” *Nature* **553**, 55–58 (2018), arXiv:1705.08371.
- [13] J E Avron, O Kenneth, and G Yehoshua, “A study of the ambiguity in the solutions to the Diophantine equation for Chern numbers,” *Journal of Physics A: Mathematical and Theoretical* **47**, 185202 (2014).
- [14] Q Niu and D J Thouless, “Quantised adiabatic charge transport in the presence of substrate disorder and many-body interaction,” *Journal of Physics A: Mathematical and General* **17**, 2453–2462 (1984).
- [15] P.-G. de Gennes, “Soluble model for fibrous structures with steric constraints,” *Journal of Chemical Physics* **48**, 2257–2259 (1968).
- [16] P. Le Doussal and D. R. Nelson, “Statistical mechanics of directed polymer melts,” *EPL (Europhysics Letters)* **15**, 161 (1991).
- [17] Randall D. Kamien, Pierre Le Doussal, and David R. Nelson, “Theory of directed polymers,” *Phys. Rev. A* **45**, 8727–8750 (1992).
- [18] David R Nelson, “Defects and geometry in condensed matter physics,” (Cambridge University Press, 2002) Chap. 9.
- [19] D. Zeb Rocklin, Shina Tan, and Paul M. Goldbart, “Directed-polymer systems explored via their quantum analogs: Topological constraints and their consequences,” *Physical Review B* **86**, 165421 (2012).
- [20] D. Zeb Rocklin and Paul M. Goldbart, “Directed-polymer systems explored via their quantum analogs: General polymer interactions and their consequences,” *Physical Review B* **88**, 165417 (2013).
- [21] Sam F Edwards, “The statistical mechanics of polymers with excluded volume,” *Proceedings of the Physical Society* **85**, 613 (1965).
- [22] P G De Gennes, “Some conformation problems for long macromolecules,” *Reports on Progress in Physics* **32**, 304 (1969).
- [23] Mark W. Matsen, “Self-Consistent Field Theory and Its Applications,” in *Soft Matter Vol. 1*, Vol. 1 (Wiley-VCH Verlag GmbH & Co. KGaA, Weinheim, Germany, 2006) pp. 87–178.
- [24] M Girardeau, “Relationship between Systems of Impenetrable Bosons and Fermions in One Dimension,” *Journal of Mathematical Physics* **1**, 516 (1960).
- [25] M. Z. Hasan and C. L. Kane, “Colloquium: Topological insulators,” *Reviews of Modern Physics* **82**, 3045–3067 (2010).
- [26] Z. Dogic, J. Zhang, a. W C Lau, H. Aranda-Espinoza, P. Dalhaimer, D. E. Discher, P. a. Janmey, Randall D. Kamien, T. C. Lubensky, and a. G. Yodh, “Elongation and Fluctuations of Semiflexible Polymers in a Nematic Solvent,” *Physical Review Letters* **92**, 125503 (2004).
- [27] Heino Finkelmann, Dieter Naegel, and Helmut Ringsdorf, “Orientation of nematic liquid crystalline polymers in the electric field,” *Die Makromolekulare Chemie* **180**, 803–806 (1979).
- [28] T. L. Morkved, M. Lu, A. M. Urbas, E. E. Ehrichs, H. M. Jaeger, P. Mansky, and T. P. Russell, “Local control of microdomain orientation in diblock copolymer thin films with electric fields,” *Science* **273**, 931–933 (1996).
- [29] R. D. King-Smith and David Vanderbilt, “Theory of po-

- larization of crystalline solids,” *Physical Review B* **47**, 1651–1654 (1993).
- [30] Raffaele Resta, “Macroscopic polarization in crystalline dielectrics: the geometric phase approach,” *Reviews of Modern Physics* **66**, 899–915 (1994).
- [31] Raffaele Resta, “Quantum-Mechanical Position Operator in Extended Systems,” *Physical Review Letters* **80**, 1800–1803 (1998).
- [32] Raffaele Resta, “Manifestations of Berry’s phase in molecules and condensed matter,” *Journal of Physics: Condensed Matter* **12**, R107–R143 (2000).
- [33] A. Bruno-Alfonso and D R Nacbar, “Wannier functions of isolated bands in one-dimensional crystals,” *Physical Review B* **75**, 115428 (2007).
- [34] J. Zak, “Berry’s phase for energy bands in solids,” *Physical Review Letters* **62**, 2747–2750 (1989).